# INVESTIGATION OF RESIDUAL STRESSES
# IN TANK CAR SHELLS
# IN THE VICINITY OF WELD ENDS

**Jeff Gordon**
**Brian P. Marquis**
**David Y. Jeong**
US Department of Transportation
John A. Volpe National Transportation Systems Center
Cambridge, MA  02142  USA


**A. Benjamin Perlman**
Tufts University
Medford, MA  02155  USA

## ABSTRACT

A large number of cracks which develop in railroad tank car shells form near the ends of skip welds which are used to attach stiffeners to the tank.  The development and growth of these cracks in fatigue are affected by the presence of residual stresses induced locally in the shell plate by welding.  Leaking and the potential for tank failure pose significant safety concerns, especially in the case of tank cars containing hazardous materials.   Determination of the distribution and magnitude of these residual stresses is important in assuring the structural integrity of tank shells.  A three-dimensional thermo-elastic-plastic finite element model (FEM) of a skip weld has been developed to explore the residual stress distribution in the weld and the surrounding base material.  The model geometry corresponds to that used in a series of experiments designed to measure residual stresses by means of X-ray and neutron diffraction.  Model results are presented for characteristic skip welds on base plates of standard tank shell material and comparisons are made between the model predictions and the laboratory measurements.  Validation of the model will permit its use in evaluating residual stresses in the vicinity of different weld geometries used for other tank shell attachments.

## INTRODUCTION

The importance of residual stresses in the vicinity of welds was identified during a task force assessment of non-conforming intermittent attachment (skip) welds discovered on certain hazardous material (HAZMAT) tank cars by Federal Railroad Administration (FRA) inspectors.  This welding technique is used  for attachments to tank car shells to permit breakaway of the attached stiffener before causing damage to the shell.   After resolution of the original problem, the project continued in order to develop a rational basis for estimating the effects of attachment welds on the structural integrity of tank car shells.

A simplified theoretical model was  developed to support the task force assessment (Orringer, et al., 1988).  The findings from this study indicated that significant tensile residual stresses were expected in the shell, near the ends of the skip welds.  The presence of such stresses would encourage the formation and growth of fatigue cracks in this area.   To determine the validity of the preliminary estimates, the Oregon Graduate Institute (OGI), under a research grant from FRA, fabricated skip-weld specimens and performed destructive tests on some of them to measure the residual stresses.  These specimens consisted of a pair of 76 mm (3 inch) welds aligned along the centerline of a $203 \times 127$ mm ($8.0 \times 5.0$ in) flat base plate separated by 51 mm (2 in) as shown in the dimensional schematic in Figure 1.  The measurements were in qualitative agreement with the estimates from the simplified model.   Blind-hole drilling measurements made at the US DOT Transportation Technology Center (TTC) at the ends of the actual attachment welds on tank car shells also confirmed the model results.

In 1994, the National Institute of Standards and Technology (NIST) conducted additional tests using specimens remaining from the OGI project (Hicho, et al., 1995).  In the NIST tests, the through-thickness distribution of residual stress was investigated by means of a combination of X-ray and neutron diffraction measurements.  The NIST results also corroborated the existence of residual tension near the weld end, and a reduction of stress through the thickness was found.  To investigate the importance of these results, a new model, using three-dimensional finite elements, was developed to simulate the end of a weld bead and the contiguous region of the base plate.   The configuration is intended to match the geometry of the specimens tested by NIST, in order to facilitate model calibration.   Once validated, the model will be used to study the sensitivity of base plate residual stress to parameters that could be controlled by design or shop practice.

## IMPLEMENTATION

A thermo-mechanical analysis of a skip welded plate was performed to estimate the residual stress state in the base plate in the region ahead of a skip weld tip. A three-dimensional model was constructed since the goal was to determine the lateral and through-thickness distributions of stress in the plate. The dimensions of the weld bead are assumed to be known a priori. Symmetry of the bead and base plate combination is assumed along a longitudinal plane through the bead and for planes perpendicular to the bead at its midpoint and halfway between the bead tips. The entire bead is treated as if it were created instantaneously on the plate. A decoupled heat transfer and stress analysis of the quarter-symmetric bead on plate is conducted as the bead cools from its laying temperature. The transient temperatures are loads for the mechanical analysis to compute the stresses that remain in the plate when the entire structure reaches the ambient temperature.
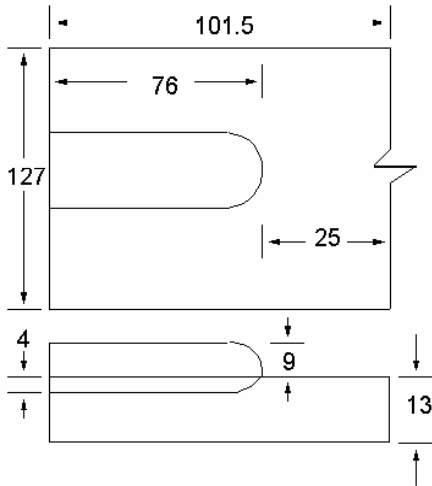


**Figure 1:  Schematic representation of one-half of the plate specimen.  Dimensions in mm (25.4 mm = 1 inch).**

## THERMAL MODEL DESCRIPTION

TOPAZ3D, an implicit finite element computer code developed at the Lawrence Livermore National Laboratory (LLNL) for heat transfer analysis (Shapiro, 1985) was used to solve the nonlinear transient heat transfer problem. The tip of the bead, the region in which the highest stress gradients occur, is the area of greatest interest and determines the character of the mesh. To assess the influence of mesh density, two FEM meshes were used in the current study and are shown in Figure 2. The coarse grid has 272 brick elements and the refined mesh has 1856 brick elements. Both meshes, created using the preprocessor INGRID (Christon and Dovey, 1992), use smaller elements with better aspect ratios close to the bead tip. The weld bead is modeled as a piece at a high initial temperature, 1500°C (2732 °F), just after deposition, while the base plate is at the ambient temperature, 27°C (80 °F). The bead and base plate parts are of the same material, A515-70 steel, for which a temperature independent density of 2,700 kg/m$^3$ (168.5 lb$_f$/ft$^3$) was used. Temperature dependent specific heat $c_p$ and thermal conductivity $\lambda$ values for this

material have been adapted from Lundèn (1991) and are shown in Table 1. Since the behavior of the bead was of secondary importance, material phase or microstructural changes, latent heat release, or complicated weld pool mechanics were not considered in the present analysis.
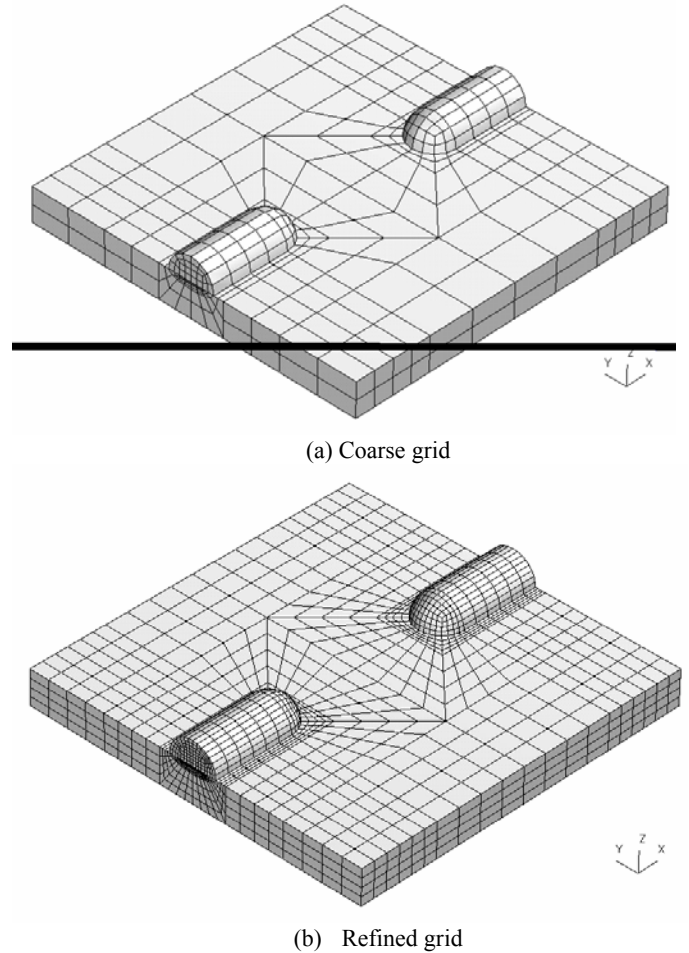


(a) Coarse grid



(b)   Refined grid

**Figure 2:  Finite element meshes used in the current study. For analysis, a quarter-symmetric representation is used.**

**Table 1: Thermal property data for A515-70 steel.**

| Temperature (°C) | Specific Heat $c_p$ (J/kg K) | Thermal Conductivity $\lambda$ (W/m K) |
|---|---|---|
| 0 | 419.5 | 59.7 |
| 300 | 588.0 | 46.7 |
| 500 | 638.4 | 38.0 |
| 700 | 649.5 | 29.2 |
| 1000 | 666.1 | 27.7 |
| 1300 | 682.9 | 31.8 |
| 1600 | 699.6 | 35.9 |

As heat transfer begins, the bead initially cools rapidly as conduction into the base plate (governed by the material properties described above) takes place, resulting in steep thermal gradients in the base plate. This non-uniform thermal expansion leads ultimately to the formation of residual stresses in the workpiece upon cooling due to shrinkage of the bead on the stiffer base plate. Heat transfer by convection from the top surface of the bead, the top and bottom surfaces of the plate, and the outer edge of the plate is represented by temperature-dependent convection coefficients which range from 1 to 13 $W/m^2 K$. Radiation from the top surface of the bead is taken into account using a constant coefficient of $5.39 \times 10^{-8}$ $W/m^2 K^4$, the product of the Stefan-Boltzmann constant and the surface emissivity. No heat transfer is permitted along planes of symmetry.

Relatively small time steps (0.05 s for the first 20 s) are needed to capture the thermal gradients which develop as cooling is initiated. As the calculation progresses, the time step is increased (5.0 s from 20.0 to 200.0 s and 50 s thereafter). The analysis is terminated at 4000 seconds (about 1 hour) when the bead and the plate have cooled to ambient temperature.

## MECHANICAL MODEL DESCRIPTION

NIKE3D (Maker, 1995), a companion code to TOPAZ3D, uses the transient temperature distributions predicted during the heat transfer analysis to compute the residual stresses.

In this analysis, the following material properties are temperature-dependent: Young's modulus $E$, Poisson's ratio $\nu$, secant coefficient of thermal expansion (CTE) $\alpha_s$, yield strength $\sigma_{YS}$ and plastic hardening modulus $E^p$. The stress-strain curve is assumed to be thermo-elastic-plastic. Table 2 lists the assumed values for A515-70 steel, adapted from Lundèn (1991). The $\alpha_s$ are defined for the bead and the plate with respect to their high and low initial temperatures, respectively (Maker, 1995).

**Table 2: Mechanical property data for A515-70 steel.**

| Temp. (°C) | Young's Modulus $E$ (MPa) | Poisson's Ratio $\nu$ | Secant CTE $\alpha_s$ $\times 10^{-5}$ $T_{ref}$ 27°C | Secant CTE $\alpha_s$ $\times 10^{-5}$ $T_{ref}$ 1500°C | Yield Strength $\sigma_{YS}$ (MPa) | Tangent Modulus $E^p$ (MPa) |
|---|---|---|---|---|---|---|
| 0 | 229000 | 0.275 | 0.996 | 1.58 | 261 | 22900 |
| 300 | 198000 | 0.290 | 1.14 | 1.70 | 248 | 23760 |
| 500 | 179000 | 0.302 | 1.23 | 1.76 | 234 | 12530 |
| 700 | 166000 | 0.310 | 1.31 | 1.82 | 225 | 3320 |
| 1000 | 147000 | 0.322 | 1.42 | 1.91 | 212 | 2940 |
| 1300 | 128000 | 0.334 | 1.52 | 2.00 | 198 | 2560 |
| 1600 | 109000 | 0.346 | 1.61 | 2.09 | 185 | 2180 |

For the mechanical analysis, displacement constraints account for the symmetry conditions. On the x-z plane along the centerline of the weld, displacement is constrained in the y-direction; for the y-z plane between the two bead tips, no x-displacement is allowed. A condition of generalized plane strain is enforced on the y-z symmetry plane which bisects the bead transversely. All of the nodes on this plane are constrained to have the same x displacement.

## RESULTS AND DISCUSSION

Figure 3, the temperature time histories at four positions along the weld centerline, indicates the thermal gradients at the plate surface in the region of interest. After 20 seconds of cooling, temperatures throughout the bead and base plate differ by at most 100 °C (212 °F), and no further significant changes in the residual stress distribution will occur. Results obtained during the first twenty-second segment only are presented here.

At the point inside the bead (point D), the cooling rate is extremely rapid as the temperature is reduced by 1300 °C (2372 °F) during the first 10 seconds. No experimental measurements are available for this weld geometry to corroborate this estimate. This cooling rate is somewhat higher than that reported for butt-welded plates (Tekriwal and Mazumder, 1988). However, the predicted residual stresses have been shown to be independent of the cooling rate (Welding Research Council, 1993).
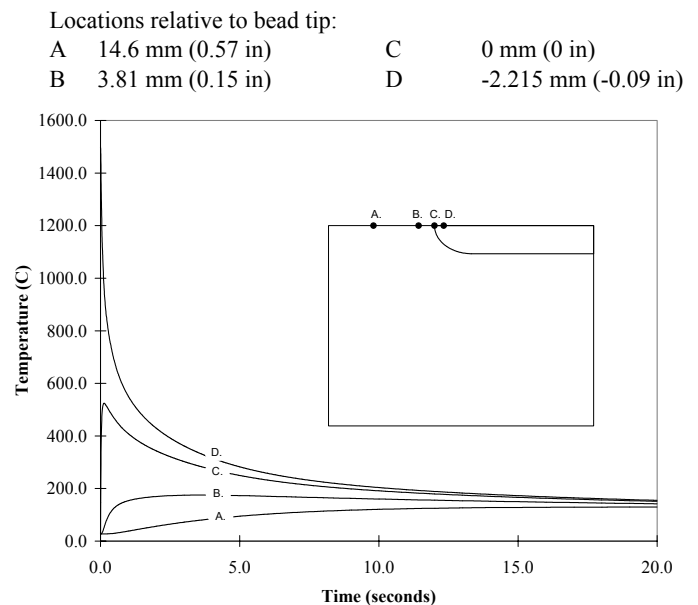
Locations relative to bead tip:

| A | 14.6 mm (0.57 in) | C | 0 mm (0 in) |
|---|---|---|---|
| B | 3.81 mm (0.15 in) | D | -2.215 mm (-0.09 in) |



**Figure 3: Temperature time history on top surface (refined grid).**

The propagation of heat from the bead into the plate is illustrated in Figure 4, which shows isotherms on the top surface of the plate at different times during cooling. After 1.25 seconds, Figure 4 (a), the bead has started to cool and the temperature in the base plate in the region surrounding the bead increases. By 5.0 seconds, Figure 4 (b), the thermal gradients in the bead and base plate have diminished. Sometime after 5.0 seconds the temperature in the bead reaches that of the surrounding plate and further heating of the plate ceases. At this point the bead and plate cool together. Figure 4 (c) shows the temperature at 20.0s.
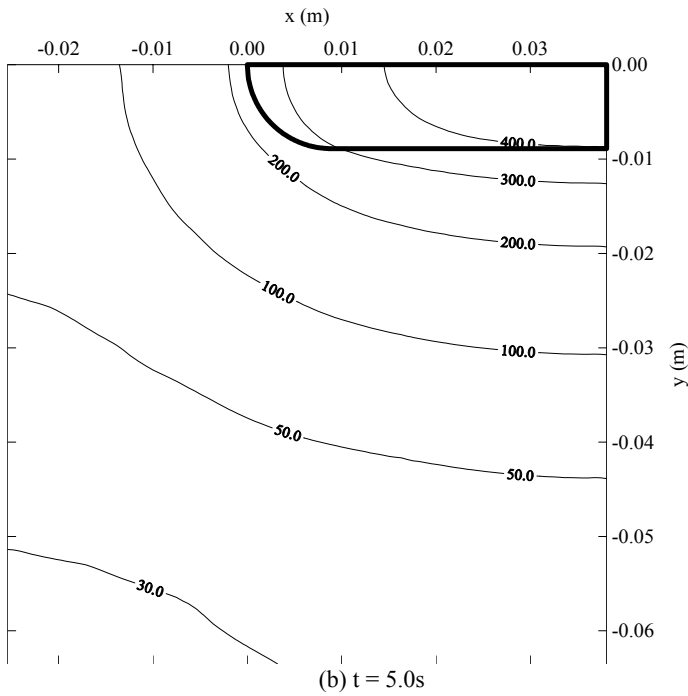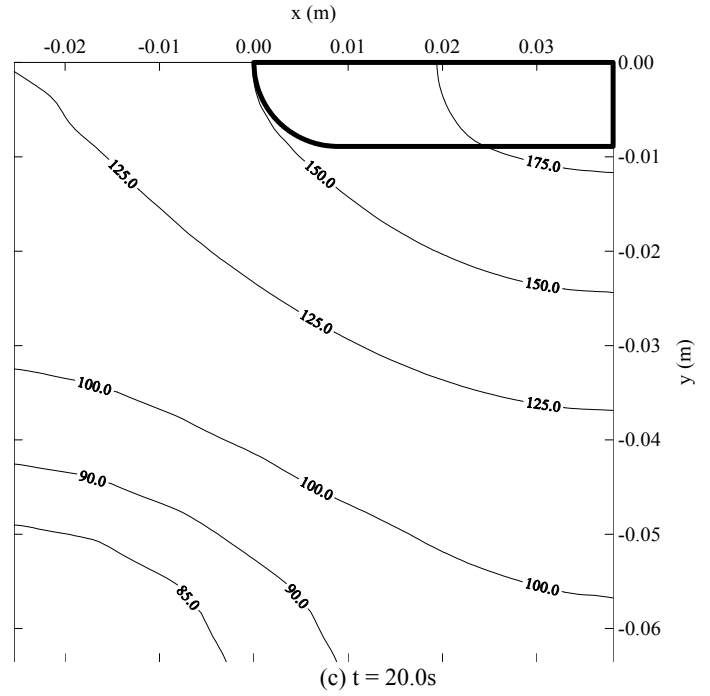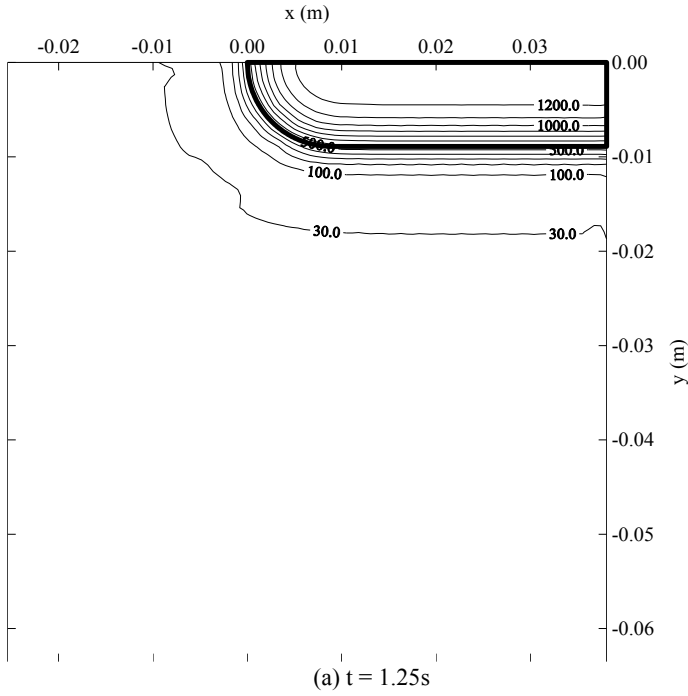
x (m)

-0.02    -0.01    0.00    0.01    0.02    0.03

(a) t = 1.25s

x (m)

-0.02    -0.01    0.00    0.01    0.02    0.03

(c) t = 20.0s

**Figure 4: Temperature contours on the top surface of the plate (°C) at different times during cooling (refined grid).**

After 20 seconds of cooling, the state of stress in the plate has stabilized. Figure 5 shows contours of the longitudinal stress on the top surface of the plate. Solid contours represent tensile (+) or zero stress and dashed lines indicate contours of compressive (-) stress. The maximum tensile longitudinal stress in the base plate, shown in Figure 5 (a), occurs ahead of the bead, and decreases with distance from the tip. The transverse stress is also tensile at the tip and out to about 5 mm along the centerline after which it becomes compressive. The maximum value of the transverse stress is also at the tip of the bead. This biaxial tensile residual stress field would encourage growth of fatigue cracks in this area and reinforces the earlier predictions (Orringer, et al., 1988).
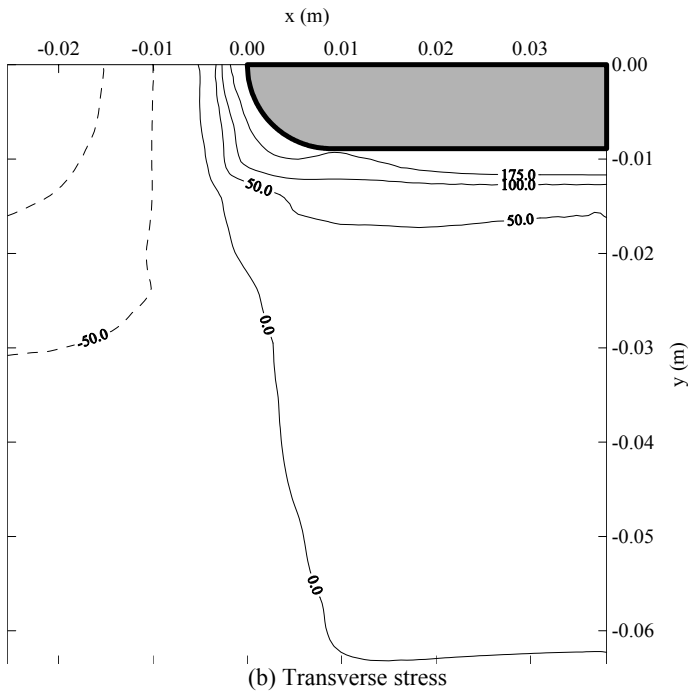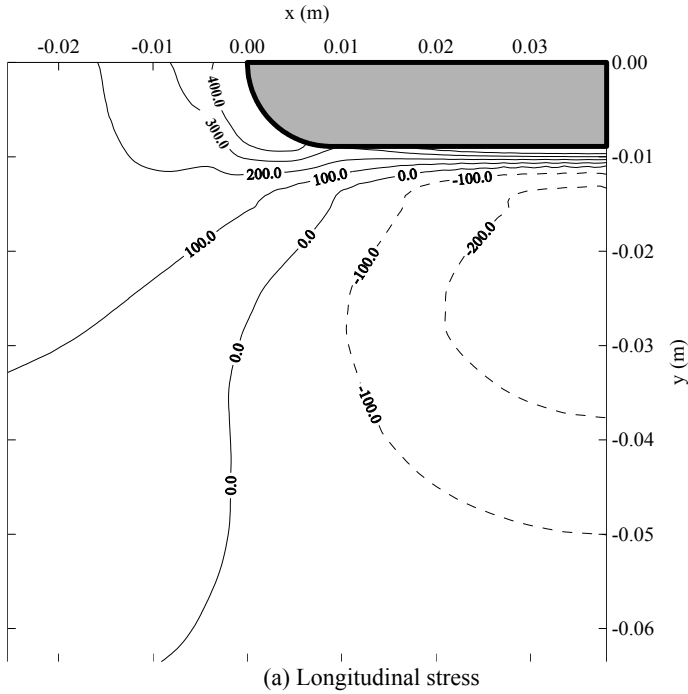
x (m)

-0.02    -0.01    0.00    0.01    0.02    0.03

(b) t = 5.0s

(a) Longitudinal stress



(b) Transverse stress

**Figure 5: Contours of stress (MPa, 1 ksi = 6.895 MPa) on the upper surface of the plate at t = 20 s (refined grid).**

A comparison of the current estimates with previous results obtained by a simplified Green's function approximation of base plate residual stresses (Orringer, et al., 1988) is shown in Figure 6. Figure 6 (a) depicts predictions of longitudinal residual stress along a line perpendicular to the weld centerline 1.5 mm (0.06 in) ahead of the weld bead at the surface of the plate and 3, 6 and 9 mm (0.12, 0.24, and 0.35 in) below the surface. Figure 6 (b) illustrates the comparison for the transverse stress component. The earlier estimates are based on the assumptions that the bead is stressed to its ultimate strength $U$ during cooling and the ends of skip welds can be treated as concentrated loads $P$ equal to $UA$ (where $A$ is the cross-sectional area of the bead) acting on the surface of the plate. Stresses in the plate are obtained by superposing the membrane stresses induced by the midplane force $P$ and the bending stresses created by the moment $Pt/2$ (where $t$ is the plate thickness) to account for the fact that the load is offset to the plate surface. Green's function approximations for the bending component are scaled to obtain estimates through the plate thickness. The agreement between the two results is encouraging. The only significant difference in the distributions is in the region immediately ahead of the weld bead tip. This is not surprising, as the simplified approximation is one-dimensional, and plate stresses at a point are estimated based upon the distance of the point from the concentrated load. The Green's function approximation suffers from a numerical singularity as this distance approaches zero, which can be seen in Figure 6 (a) and (b). Both results indicate biaxial tension in the region immediately ahead of the bead tip at the plate surface, although the relative magnitudes differ.



(a)   Longitudinal stress
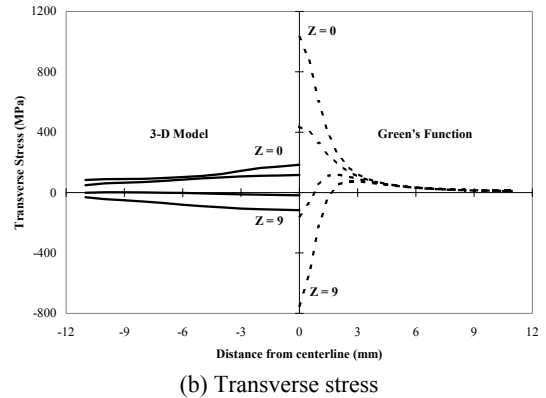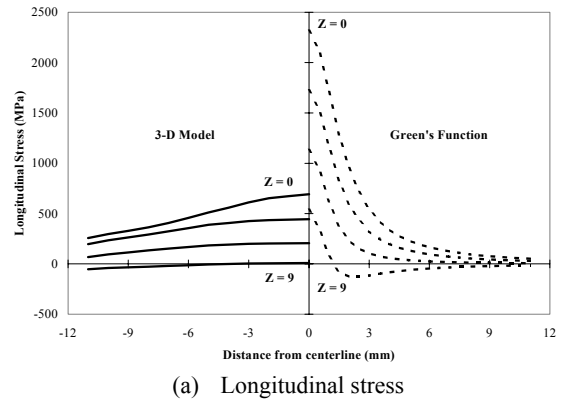


(b) Transverse stress

**Figure 6: Comparison of Green's function approximation and 3-D model results for plate residual stress on line perpendicular to weld centerline 1.5 mm in front of bead tip and at different depths, z, from the plate surface.**

The measurements using the neutron diffraction technique were made at locations identified with round black dots in Figure 7. This set of experiments focused on the longitudinal distribution in front of the bead. These points begin 1.5 mm (0.06 in) along the centerline in front of the bead tip and are spaced 3 mm (0.12 in) apart. The measurements are taken at depths of 3, 6, and 9 mm (0.12, 0.24 and 0.35 in) from the upper surface of the plate. Another series of measurements were taken on a plane perpendicular to the plate centerline and 1.5 mm in front of bead tip. These points are located at 3, 6 and 11 mm (0.12, 0.24 and 0.43 in) from the centerline at the same depths. Measurements were made on four samples representing variations in shielded metal arc welding (SMAW) parameters which include: the applied welding current, the travel speed, and the leading angle of the electrode with respect to the plate normal. As the current model does not account for these effects, the residual stress measurements at each point are averaged for the eight samples (four specimens with two welds on each) for comparison with the FEM predictions.
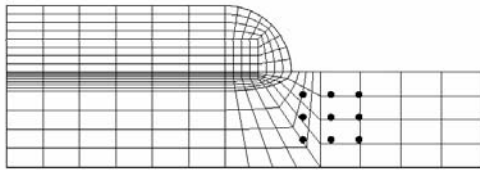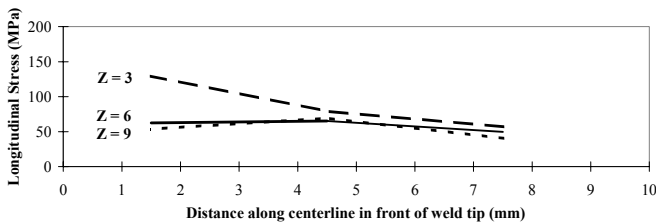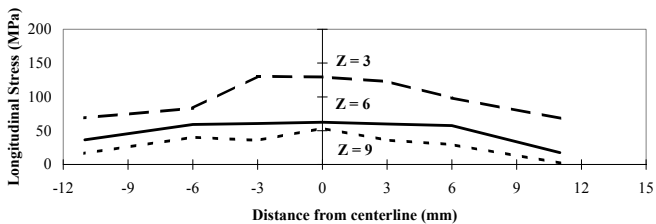


**Figure 7: Location of experimental measurements relative to bead tip.**

To improve the clarity of subsequent comparisons, the experimental measurements are first presented alone, Figure 8. In Figure 8 (a), the measurements, made along the bead centerline
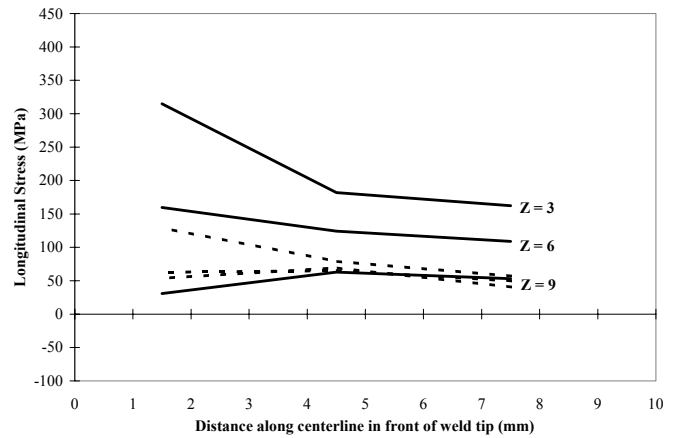


(a) Along bead centerline in front of bead tip



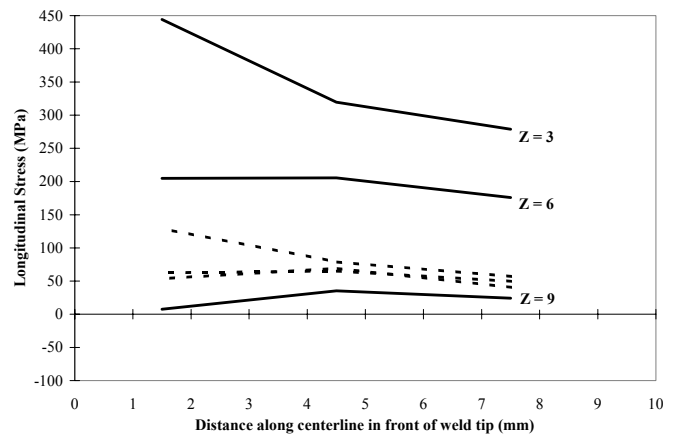(b) Along line perpendicular to bead centerline, 1.5 mm ahead of tip

**Figure 8: Measured longitudinal residual stress at different depths, z, from the plate surface.**

correspond to the locations in Figure 7. It should be noted that there was wide variation in the experimental data with a standard deviation ranging from 24.4 to 54.4 MPa (3.5 to 8 ksi). Figure 8 (b) shows the measurements taken on a plane perpendicular to the plate centerline and 1.5 mm in front of bead tip. This data also had a large variation, ranging from 17.6 to 59.6 MPa (3 to 9 ksi). In subsequent figures, which compare predicted results to experimental data, the measured results appear as dashed lines.

A comparison of the longitudinal residual stress measurements and the corresponding model predictions are shown in Figure 9. Qualitatively, the model shows trends quite similar to those of the experiment. However, the computed values for tensile residual stress are significantly higher. These differences are more pronounced in the results obtained using the refined grid. The influence of gradients near the tip is reflected in the values further away from the bead.



(a) Coarse grid



(b) Refined grid

**Figure 9: Comparison of measured (dashed) and predicted (solid) longitudinal residual stress at locations along base plate centerline in front of bead tip and at different depths, z, from the plate surface (t = 20.0 seconds).**

A comparison of the predicted and measured longitudinal residual stress along a line perpendicular to the base plate centerline and 1.5 mm (0.06 in) from the bead tip is shown in Figure 10. The trends are very similar. The model results vary roughly linearly through the plate thickness. In regions of the plate remote from the effects of the weld tip the stress through the thickness is nearly constant, around 20 MPa (2.9 ksi). The lateral extent of the tensile zone is dictated by the width of the bead. For a thinner bead, there would be a sharper tensile peak and the breadth of the distribution would be narrower (more like the Green's function approximation).

studied by performing an additional analysis with no constraint on the y-z symmetry plane. There was no change in the stresses ahead of the tip although there were differences in the far-field residual stresses.

The effect of CTE and yield strength on the model predictions was examined by varying their values over a range that reflects the uncertainty in these properties. The secant CTE was decreased by 25% to more closely correspond to values specified by the Association of American Railroads (AAR, 1984). Figure 11 shows the longitudinal residual stress resulting from this change. The reduction in CTE leads to a similar reduction in the peak value of residual stress, from 351 MPa (46 ksi) to 259 (38 ksi). These predictions are in closer agreement with the experimental measurements. When a similar variation was applied to the temperature dependence of the yield strength, the distribution in the region of interest was essentially unchanged, Figure 12.



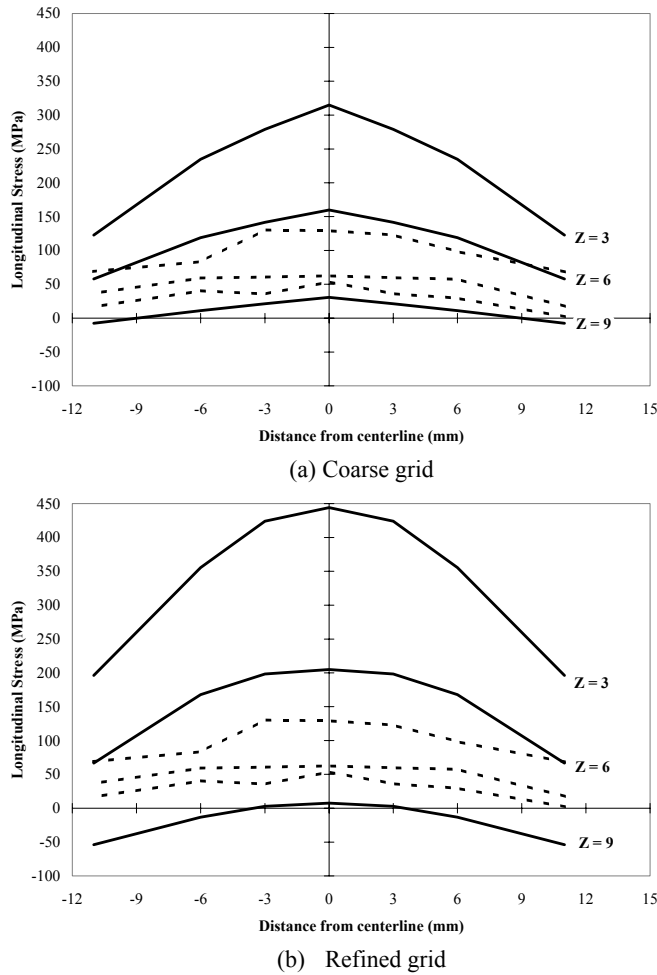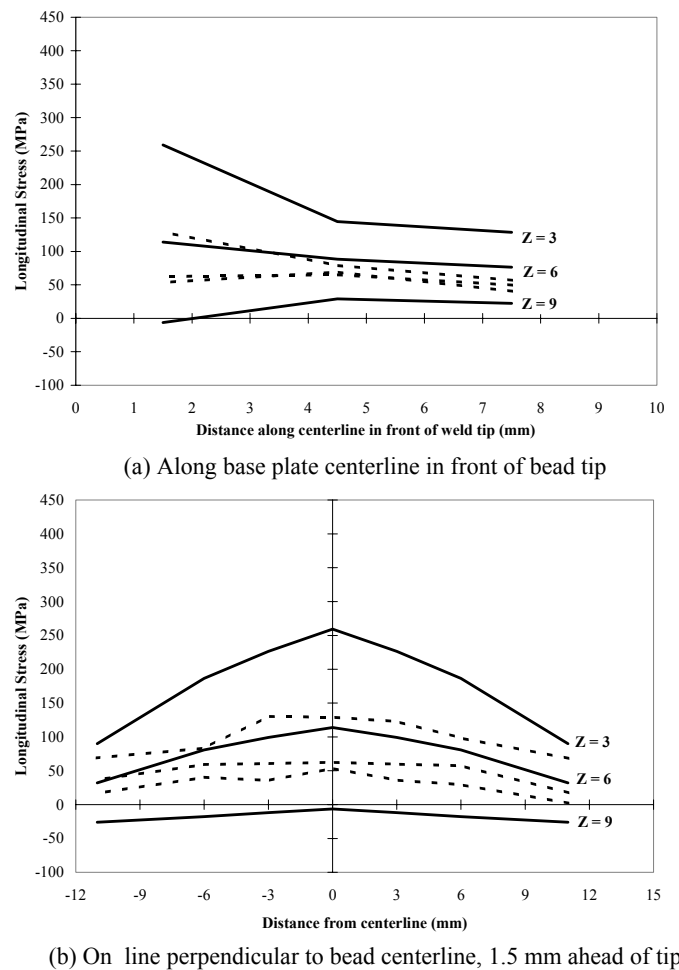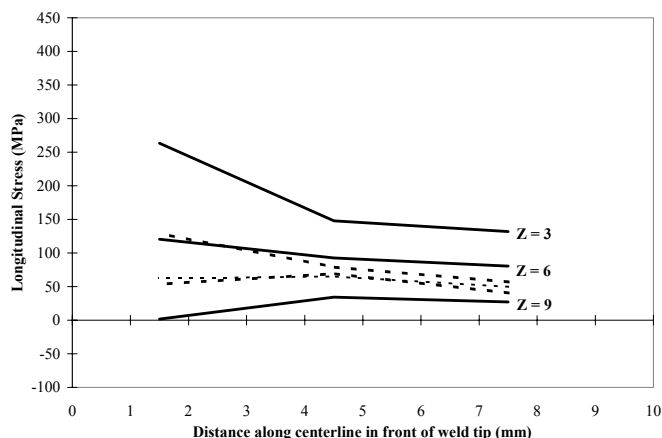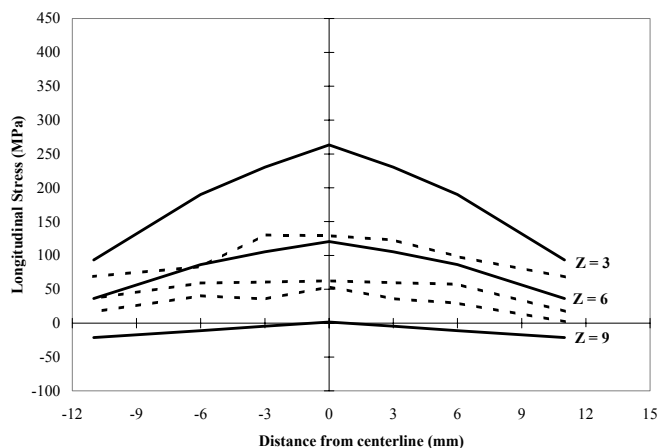(a) Coarse grid



(b) Refined grid

**Figure 10: Comparison of measured (dashed) and predicted (solid) longitudinal residual stress on line perpendicular to base plate centerline 1.5 mm in front of bead tip and at different depths, z, from the plate surface (t = 20.0 seconds).**

The parameters chosen to characterize the material behavior, the initial conditions and the boundary constraints determine the magnitude of the predicted stresses. In terms of material behavior the yield strength, Young's modulus, and CTE have the largest influence on the results. The effect of the generalized plane strain condition was



(a) Along base plate centerline in front of bead tip



(b) On line perpendicular to bead centerline, 1.5 mm ahead of tip

**Figure 11: Comparison of measured (dashed) and predicted (solid) longitudinal residual stress using modified CTE at different depths, z, from the plate surface (t = 20.0 seconds); coarse grid.**

(a) Along base plate centerline in front of bead tip



(b) On  line perpendicular to bead centerline, 1.5 mm ahead of tip

**Figure 12: Comparison of measured (dashed) and predicted (solid) residual stress using modified CTE and modified yield strength at different depths, z, from the plate surface (t = 20.0 seconds); coarse grid.**

## CONCLUSIONS

The preliminary results for longitudinal residual stresses in a base plate in the vicinity of the tip of a weld reported here are in qualitative agreement with laboratory measurements. With additional refinements, the three-dimensional finite element model can provide a rational basis for estimating the effect of attachment welds on tank car structural integrity. The model has demonstrated that boundary constraints and heat transfer aspects have relatively small effects. Several factors which could influence the results require further examination. Among these are the geometry of the bead (its size and shape, initial temperature) and the high-temperature material properties for the material. The reference values for these parameters were chosen in this study to provide conservative estimates of plate residual stresses. It has been shown that the effects of changes to material properties have no significant impact on the predicted residual stress distribution except for the assumed value of the CTE.

In addition, the estimates from the three-dimensional model presented here neglect the presence of initial residual stresses in the plate. A previous study examined the development of through-thickness residual stresses in a thick plate subject to surface quenching after hot-rolling (Gordon and Orringer, 1995), and indicated that significant residual compression can be induced on the surface of a plate depending on the severity of the quench. The effect of initial residual compression from manufacturing is likely to reduce the magnitude of the residual tension on the plate surface.

## ACKNOWLEDGMENT

## REFERENCES

Association of American Railroads, 1984. Manual of Standards and Recommended Practices, Section G, Standard S-660-83, "Procedure for the Analytic Evaluation of Locomotive and Freight Car Wheel Designs," p. G-62.

Christon, M. A., and Dovey, D., 1992, "INGRID A 3-D Mesh Generator for Modeling Nonlinear Systems, User Manual," Methods Development Group, Lawrence Livermore National Laboratory, UCRL-MA-109790 Draft.

Gordon, J.E. and Orringer, O., 1995, "Prospects for making carbide-free bainitic thick steel plate by means of controlled quenching: a first estimate," *International Mechanical Engineering Congress and Exposition*, R.R. Newman, ed., American Society of Mechanical Engineers, New York, RTD Vol. 10, pp. 119-126.

Hicho, G. E., Brand, P. C., and Prask, H. J., 1995, "Determination of the Residual Stresses Near the Ends of Skip Welds Using Neutron Diffraction and X-Ray Diffraction Procedures," US Department of Commerce, National Institute of Standards and Technology, NISTIR 5671, Report No. 29, Gaithersburg, MD.

Lundèn, R., 1991. Contact region fatigue of railway wheels under combined mechanical rolling pressure and thermal brake loading. In *Wear* 144, pp. 57-70.

Maker, B. N., 1995, "NIKE3D A Nonlinear, Implicit, Three-Dimensional Finite Element Code for Solid and Structural Mechanics - User's Manual," Methods Development Group, Lawrence Livermore National Laboratory, UCRL-MA-105268 Rev. 1.

Orringer, O., Gordon, J.E., Tang, Y.H. and Perlman, A.B., 1988, "On some problems of stress concentration in tank car shells," *Applied Mechanics Rail Transportation Division Symposium,* H.H. Bau, T. Herbert, and M. Yovanovich, ed., American Society of Mechanical Engineers, New York, RTD Vol. 2, pp. 87-94.

Shapiro, A. B., 1985, "TOPAZ3D - A three-dimensional finite element heat transfer code, User's Manual," Methods Development Group, Lawrence Livermore National Laboratory, UCID-20484.

Tekriwal, P., and Mazumder, J., 1988, "Finite Element Analysis of Three-Dimensional Transient Heat Transfer in GMA Welding," *Welding Journal*, Vol. 76, No. 7, pp. 150s-156s.

Welding Research Council, 1993, "Non-destructive Measurement and Analysis of Residual Stress in and around Welds-A State of the Art Survey," *Welding Research Council Bulletin* 383.